High Accuracy Calibration of Photon-Counting Detectors

Sergey V. Polyakov[*a], Michael Ware[b], and Alan Migdall[a]

[a] Optical Technology Division, National Institute of Standards and Technology, 100 Bureau Drive,
Gaithersburg, MD 20899-8441 and
Joint Quantum Institute, Univ. of Maryland, College Park, MD 20742
[b] Dept. of Physics and Astronomy, Brigham Young Univ., N283 ESC
Provo, UT 84602

ABSTRACT

We discuss a practical implementation of a photon-counting detector calibration using correlated photon pairs produced by parametric down-conversion. In this calibration scheme, the detection of a first photon triggers the measurement sequence aimed at detection of a second photon by a detector under test (DUT). We also describe measurements of radiant power with a photon-counting detector, which is important for implementation of a conventional calibration technique based on detector substitution. In the experiment, we obtain a time-delay histogram of DUT detection events consisting of a correlated signal and a background. We present a method for separating the correlated signal from the background signal that appropriately handles complex properties of typical avalanche photodiode (APD) detectors. Also discussed are measurements of relevant APD properties, including count-rate-dependent afterpulsing, delayed (by up to 10 ns) electronic detections and deadtime effects. We show that understanding of these is essential to perform an accurate calibration.

Keywords: calibration, detector, down-conversion, correlated photons, statistical methods

1. INTRODUCTION

We review several techniques and algorithms used in a practical implementation of high accuracy single photon detector (SPD) calibration. SPD calibration can be accomplished using both conventional methods (based on detector substitution) and correlated photon methods. In a conventional calibration, the radiant power of a source is measured with a SPD and then compared with a measurement made using a regular photodiode that has been independently calibrated for high accuracy radiant power measurements. In a correlated photon calibration, photon pairs are produced by a parametric downconversion (PDC) process and the two individual photons are directed to separate detectors. Because the PDC photons are produced in pairs, the detection of one photon heralds with certainty the existence of the other. Failure to detect the first 'herald' photon of the pair does not affect the uncertainty of this measurement, even if the second photon of the pair gets detected by the SPD under test, because only the correlated output of the second detector is used. This method meets the criteria to be called a "primary standard method" [1], because it is a fundamentally absolute way to calibrate SPDs [2-15]. Because the scheme operates directly in the photon-counting regime, it is well suited to SPD calibration. Indeed, we show that in addition to directly measuring detection efficiency (DE) with high accuracy, the correlated photon calibration allows independent measurement of an SPD temporal response function, and characterization of deadtime, afterpulsing and other features of SPDs.

The correlated photon method has promised high accuracy calibration measurements since its inception. Progress has been slow, however, mainly due to real-world characteristics of the SPDs used. The primary features that must be considered in a calibration are the SPD's deadtime period, where it does not count incident photons, and its afterpulsing, which gives rise to false counts. As the uncertainty of the calibration decreases, the number of contributing effects that must be considered grows. While some uncertainties better than 1% have been reported, they have not included independent verification. In this contribution, we outline techniques and methods for overcoming difficulties of SPD metrology techniques in our effort to pursue a high-accuracy independent verification of the correlation method of calibrating SPDs.

---

[*] spoly@nist.gov; phone (301)-975-8473

2. MEASUREMENTS OF SPD AND SETUP PROPERTIES WITH CORRELATED PHOTONS

2.1 Experimental setup

The key technique used in this work to establish various properties of SPDs is based on correlated photon pair detection by two SPDs: a trigger detector, and a detector under test (DUT). In our setup an Ar^+ laser operating at 351 nm was used to pump the downconversion crystal (see Fig. 1). A windowless silicon photodetector was used as a pump power monitor. A $LiIO_3$ crystal (6 mm long) was set to produce nearly degenerate downconverted photons at ~702 nm in a non-collinear configuration with an external output angle of 1.8º. Narrowband spectral filters F_T and F_{DUT} were installed in each arm. The trigger detector, a photon-counting avalanche photodiode (APD), was set at the end of a 5 m single-mode fiber. The DUT was also a photon-counting APD mounted behind an aperture to reduce PDC light not correlated to that seen by the trigger and a lens to collect the correlated light onto the ~0.2 mm DUT active area. The DUT channel was assembled on a double X-Y translation stage that allowed movement of the whole DUT assembly (from F_{DUT} to DUT SPD) or just the DUT SPD in a transverse plane. This allowed us to investigate spatial properties of the detectors as well as of the correlated photons. The detector signals were sent to a circuit that recorded both the overall number of trigger and DUT events, and the correlation between trigger and DUT events in a form of a histogram (Fig. 2) with 0.1 ns temporal resolution. This histogram contains information on several DUT properties that must be identified and quantified before the calibration can take place. This setup can be used to make calibration measurements using both the correlated and the detector substitution methods (with proper alignment and slight modification).
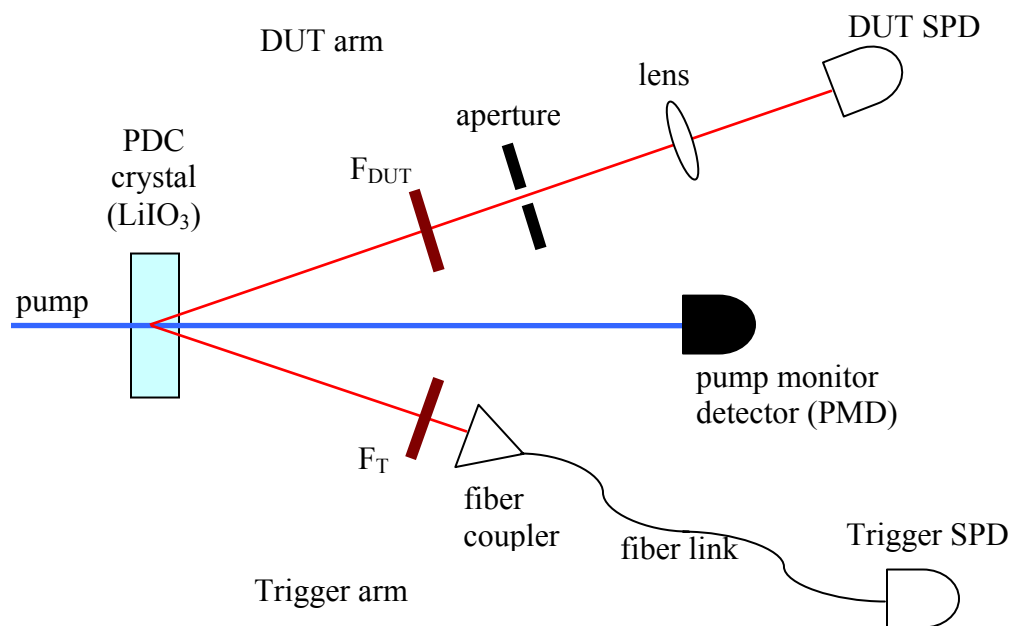
Fig. 1. Experimental setup.

2.2 Histogram features

The correlated signal is recorded as a histogram that exhibits some important properties of APDs and their temporal characteristics. As seen in Fig. 2, the correlated peaks reside on a background that corresponds to random detections. The principal coincidence peak (A) contains true coincidences, and would be the only feature visible if detectors were "ideal". The full width at half maximum (FWHM) of this peak is given by a convolution of temporal responses of both the Trigger and DUT SPDs. The total number of coincidences in this peak can be used to compute a good first-order

estimate of the DE of SPD DUT (with an uncertainty of ~2%). However, we are interested in achieving much higher accuracy, so we need to carefully characterize the setup and detector features.
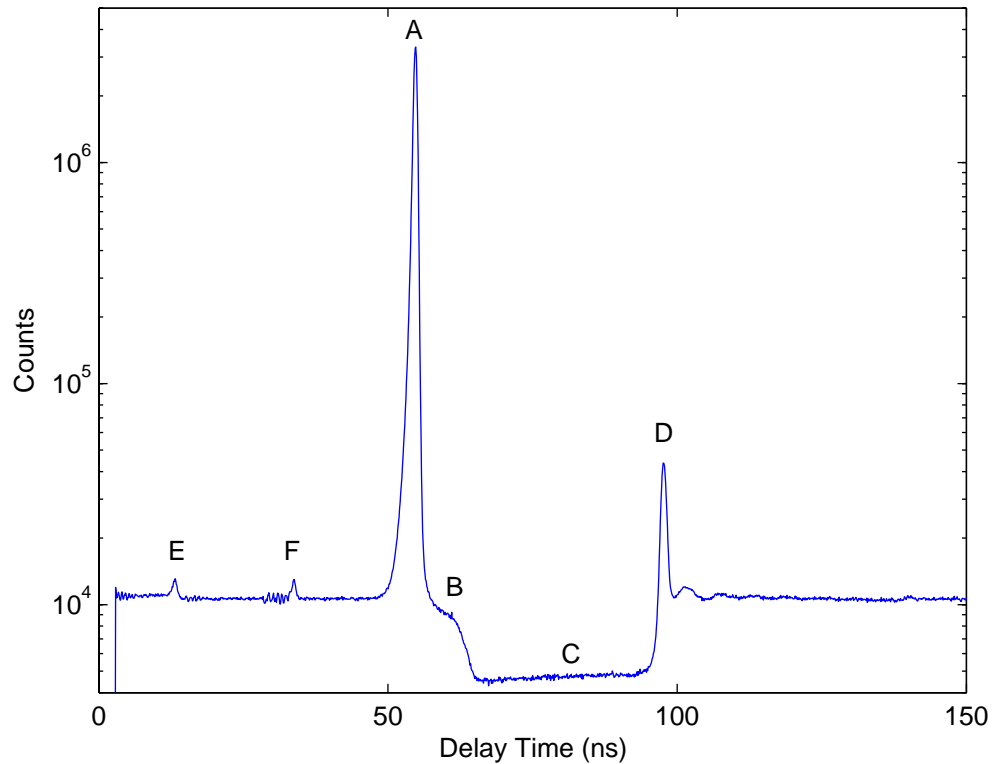
Fig. 2. Typical histogram and its main features. A – the main peak due to correlated photons, B – extended shoulder due to twilight events (see text), C – the region where the detector is dead after firing, D – peak due to afterpulsing, E – minor correlated photon peak due to afterpulsing of the trigger APD, and F – minor correlated photon peak due to double reflection in the trigger fiber.

Feature (C) is a reduction in the background rate due to the APD's deadtime, when the APD can not produce an electrical pulse even if it received a photon. We can estimate deadtime of an APD to within a couple of ns using the duration of the background reduction as well as the slight positive slope of (C). Feature (D) corresponds to detector afterpulsing. The small peaks (E) and (F) are due to trigger channel effects. Peak E is produced by afterpulsing of the trigger detector. As the second trigger restarts the histogram process for our circuitry, the correlated detections of the DUT appear 'earlier' in time than the main peak (A). Peak F is also simply understood. In our setup, we couple trigger photons into a fiber and then couple the output of the fiber onto the trigger APD. The photons that experience a reflection at both ends of the fiber arrive at the APD after traveling two extra fiber lengths, which results in detecting correlated DUT signals with shorter delays. The timing of the advance of the feature (F) is consistent with the length of the fiber used. We characterized this small double back-reflection in a separate setup and found the expected Fresnel reflections in the fiber consistent with the relative size of feature (F). The origin and significance of the feature (B) will be established later.

2.3 Separation of background

The complex nature of the background in Fig. 2 suggests that a simple background subtraction would introduce errors in the estimation of histogram features. For a more accurate treatment, we make a simple mathematical model of an SPD that deals with its essential properties such as afterpulsing and deadtime. We start with a measured histogram denoted by $H(\tau_i)$, where τ_i denotes the time delay for the ith bin. As usual, the histogram records the cumulative number of detection events received in each bin. The number of histogram trigger pulses (i.e. histogram starts) received while

accumulating the histogram is labeled by N_{trig}. Our goal is to separate the events represented by $H(\tau_i)$ into two categories: events correlated to the trigger pulse and uncorrelated background events. Formally, we write

$$H(\tau_i) = C_{\text{m}}(\tau_i) + B_{\text{m}}(\tau_i), \tag{1}$$

where $C_{\text{m}}(\tau_i)$ and $B_{\text{m}}(\tau_i)$ denote, respectively, the number of correlated and background events recorded in a given bin. The subscript 'm' reminds us that these quantities represent the number of correlated and background events that were actually measured in each bin. This is done to emphasize that there are different definitions of the detection efficiency and in a subsequent analysis $C_{\text{m}}(\tau_i)$ might need to be modified in accordance to this definition. We consider a simple model of detector deadtime where the detector is "dead" for d time bins after registering an event, and then immediately becomes live again. This deadtime treatment does not take into account minor properties of an SPD such as variation in deadtime duration and the afterpulsing after the recovery from the background count. For ease of notation, we will assume that the delay of the DUT channel has been chosen long enough so that all of the correlated signal appears after the dth histogram bin. In other words, we require that $C_{\text{m}}(\tau_i) \equiv 0,$ for $i \leq d$. We also assume that the mean number of background events in a given bin is constant before correlated events arrive, and define B_0 as the average number of background events per bin recorded in bins with $i<d$. Using B_0, we calculate the probability b that a background event could be measured in a bin (during a given scan) assuming that the detector was alive at that moment. In the absence of correlated signal, this is simply $B_0 = b(N_{\text{trig}} - B_0 d)$, where N_{trig} is a total number of trials used to record a histogram. Note the importance of the term $B_0 d$, witch gives the number of trials when the detector was dead because it fired recently (i.e. the background count was recorded in one of the d previous bins). The number in parentheses then is a total number of trials when the detector was alive and able to produce a background count. We can write a similar expression in the presence of correlated signal. In this case we have

$$B_{\text{m}}(\tau_i) = b \left[N_{\text{trig}} - \sum_{j=i-d}^{i-1} H(\tau_j) - \Delta(\tau_i) \right]. \tag{2}$$

Note that the number in brackets is the number of scans where it was possible to record a background event in the bin. The sum gives the number of times that the detector was dead in the ith bin due to a background or signal event in one of the previous d bins. The function $\Delta(\tau_i)$ accounts for the situations where a trigger pulse resets the delay before it reaches the ith bin (recall that we histogram DUT events with respect to the most recent trigger event) and provides a correction associated with afterpulsing and deadtime of a trigger detector. The shape of $\Delta(\tau_i)$ is determined by measuring a histogram with no correlated signal incident on the DUT. We can rewrite (2) using a directly measured background level B_0 as:

$$B_{\text{m}}(\tau_i) = \frac{B_0}{N_{\text{trig}} - B_0 d} \left[N_{\text{trig}} - \sum_{j=i-d}^{i-1} H(\tau_j) - \Delta(\tau_i) \right]. \tag{3}$$

Note that our definition of b does not distinguish between a background event and an afterpulse of a background event, which results in slight underestimation of the background during the dead region. We can use the background found using (3) together with (1) to determine $C_{\text{m}}(\tau_i)$, the number of correlated events measured in each bin (Fig. 3). We use $C_{\text{m}}(\tau_i)$ to calculate various properties of the SPD, including the DE [16]. Notice that feature (B) in Figs. 2 and 3 is not a part of the background, but rather a delayed correlated signal. To study the origin of this feature, we performed additional tests, described below.
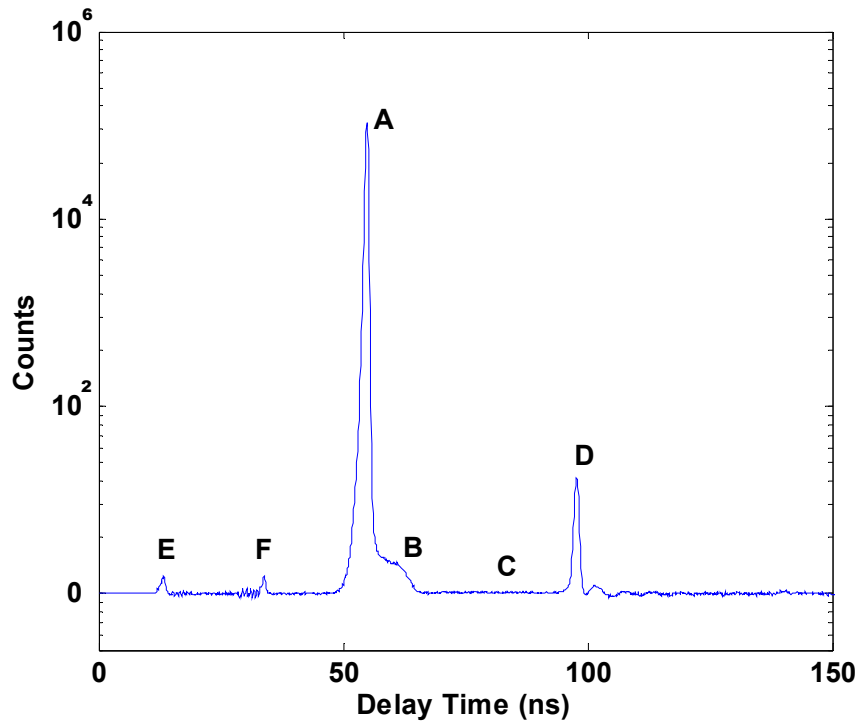
Fig. 3. Typical background subtracted histogram and its main features. A – the main peak due to correlated photons, B – extended shoulder due to twilight events (see text), C – the region where the detector is dead after firing, D – peak due to afterpulsing, E – minor correlated photon peak due to double reflection in the trigger fiber, and F – minor correlated photon peak due to afterpulsing of the trigger APD.

2.4 APD afterpulsing

An afterpulse is defined as when the APD fires (produces a count) at the end of its deadtime, associated with a previous count. We can find the afterpulse rate by analyzing the histogram (e.g. the afterpulses associated with the main peak in Fig. 3 are found in peak D). Interestingly, the rate of afterpulseing depends on the count rate (see fig. 4). By measuring the afterpulse fraction (defined as the likelihood of the detector producing a second pulse, i.e., an afterpulse, given an initial count) at a range of DUT count rates, we can quantify and fit the linear component of the afterpulse rate. We therefore conclude that the afterpulsing can be caused by a subsequent photon arriving during the last moments of the APD's deadtime (or twilight counts) [16] in addition to the usual cause of an afterpulse due to lingering trapped carriers from a previous avalanche. The line slope is proportional to the duration of the twilight period and the associated "twilight detection efficiency" (which might not be a constant throughout this interval). The zero rate intersection of this line is the rate of ordinary afterpulses. Thus at any final count rate the afterpulse peak consists of photon-related afterpulses and afterpulses, not related to a photon absorption. Note that the ordinary afterpulse fraction is a property of an APD, it varies from device to device, but stays constant in all measurements of a single APD. At the same time, the probability of getting a "twilight event" grows approximately linearly with increasing count rate. It is important to understand this difference and use a correct afterpulsing constant, whose choice is application dependent. For radiometry, we are interested in all the counts which are photon related, so most of the time we only need to quantify ordinary, "electronic" afterpulsing. Measurements of our DUT APD (fig. 4) yielded an ordinary afterpulsing fraction of (0.3218 ± 0.035) %, $k = 1$.
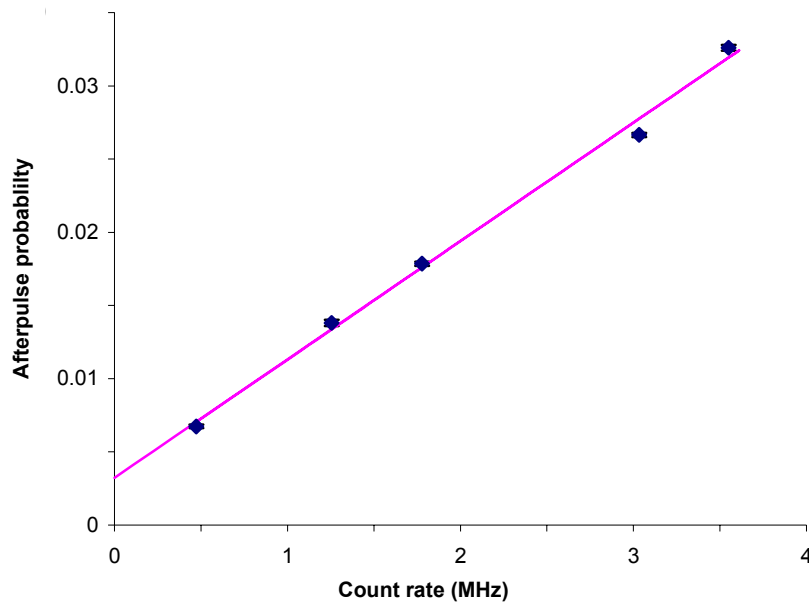
Fig. 4. Probability of the afterpulse vs. count rate (diamonds) and a best fit to a line.

2.5 Delayed electronic response of an APD

We performed a two-dimensional scan of the DUT APD's active area to establish a spatial map of delays in the electronic response of the APD. During these measurements we recorded the position (x, y) of the APD and took a histogram measurement as previously described at the count-rate of ~3MHz. We then found the location of the maximum of the main correlation peak (A) and plotted the time difference in a contour plot, Fig. 5. We observed that the electronic signal was delayed by as much as 1 ns when photons arrived near the rim of the active area as compared to the middle. Also, we see that the electronic time jitter, which is proportional to the full width at half-maximum (FWHM) of the correlation peak, increases near the rim. Note that the response is nearly radially-symmetric. Spatial maps of temporal response of the APD illustrate the feature of delayed response due to a slow diffusion of carriers from the neutral region to high electrical field region, first pointed out in [17]. These findings are interesting in their own right, and indicate that applications which call for reduced jitter should use the central portion of the APD's active area.

The origin of feature (B) in fig. 2 cannot be explained by a transverse spread of photons on the detector surface, however, since the events in (B) are delayed by ~10 ns. Figure 6 shows a set of histograms from Fig. 5 plotted versus both the time delay and the distance from the active area center. This graph clearly shows that feature (B) from fig. 2 is produced during measurements closer to the active area center, where the sensitivity and hence the count rate is the highest.

It turns out that the photon-induced APD afterpulsing discussed earlier is closely related to the delayed count feature [16]. Indeed, if the detector happened to be in its twilight mode, the photon absorption does not result in a generation of an electrical signal with the usual electronic propagation delay. Instead the electrical signal is generated after the detector becomes 'live' again. The detector stays in twilight mode for ~10 ns, in correspondence with the maximum delay in the correlated tail seen in Fig. 6.
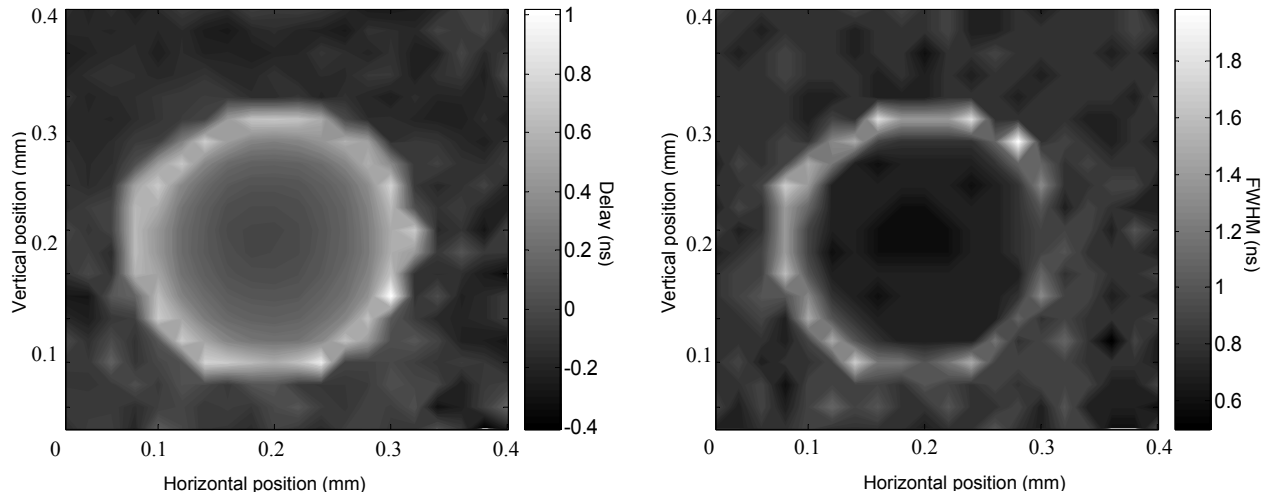
Fig. 5. Typical APD characterization maps obtained from a series of histogram measurements taken with a ~30 μm beam of correlated photons. a) Delay (ns) in the electronic output (relative to the main correlation peak) of the APD across the detector's sensitive area and b) FWHM of the main correlation peak (ns) across the detector sensitive area.
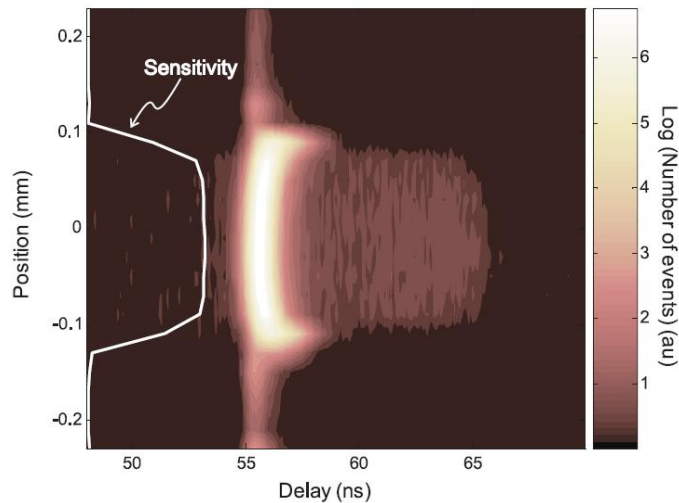
Fig. 6. APD spatiotemporal characterization map, showing the relatively small delay and electronic jitter increase at the rim of the detector and a shoulder of delayed events.

The fraction of delayed twilight counts is obviously rate-dependent. For our typical DUT count rates of ~3 Mhz, this fraction exceeds 1 % of the total correlated signal. Therefore, this effect is not negligible if one desires measurements with better than 1 % uncertainty.

The features such as rate dependent afterpulsing probability and delays in electronic response whose characterization was discussed here make it extremely difficult to achieve an accurate self-calibration i.e. calibration when one and the same detector acts as a trigger and a DUT as has been suggested by some [18].

2.6 Spatial distribution of correlated photons

The correlated photon calibration technique requires that all the photons correlated with those coupled to the single-mode fiber of the trigger arm (fig. 1) be collected by the DUT, as any geometric losses would reduce the apparent DE. By scanning the DUT arm with a small diameter (~1 mm) aperture we mapped the spatial distribution of correlated counts (fig. 7). We see a weak spot due to a double reflection from the crystal to the lower right of the main spot. The

fraction of correlated photons in this spot is ~ 1 % of the correlated photons in the main peak, in accordance with the Fresnel formula for the reflectance of the down-conversion crystal. Hence, we deduce the size of the DUT aperture (fig. 1) that should be chosen to limit the number of uncorrelated detections, while collecting all correlated photons.
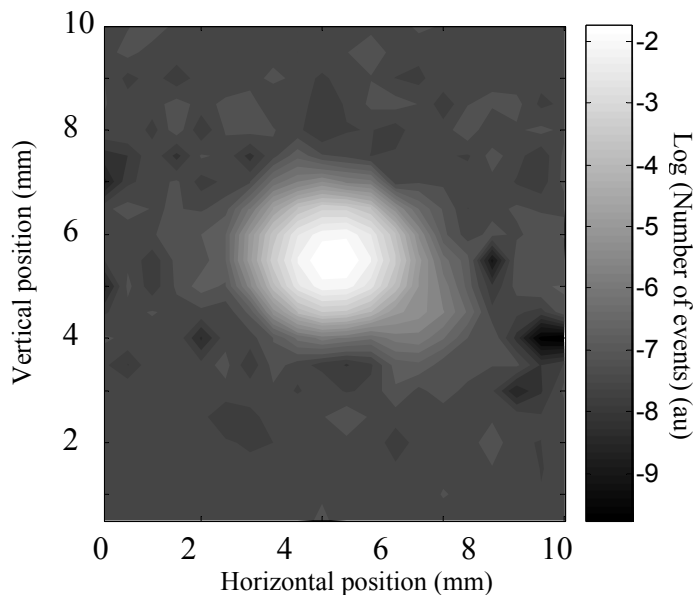
Fig. 7. Spatial map of the log of correlated counts at the DUT, as the DUT with a 1 mm aperture was scanned across the beam. (Due to noise on the background, a constant was added to the counts after background subtraction, but before taking the log.)

3. HIGH ACCURACY MEASUREMENTS OF RADIANT POWER WITH AN SPD

3.1 Definition of SPD DE

To measure radiant power with an SPD to high accuracy, we must first choose the most appropriate definition of DE. Because of the multiple features of APDs which complicate their response, the most suitable definition will depend on the application. The most common definition of DE is the fraction of the number of correlated events that would have been measured if the detector was 'live' (ready for a detection) each time a correlated photon was incident on the system, denoted by η_{live}. However, this is not always the best definition since it cannot be measured directly. Even if a value of η_{live} was provided for a detector, it could not be directly applied to a radiant power measurement of a continuous wave (cw) source, because of complex afterpulsing structure and twilight counts. Thus, we need additional information on dead time, electronic afterpulsing, twilight time and the DE of an APD in twilight 'mode'. These characteristics vary between individual detectors, but might be safely assumed not to vary with the count rate. For a cw source we could introduce an effective twilight time, which is the corrected time period so that the twilight DE can be set equal to the DE of the APD when it is 'alive'. The effective twilight time can be deduced from the slope of the linear fit in Fig. 4.

In our effort to compare the calibration technique based on correlated photon pair detection with the traditional detector substitution technique, we could improve accuracy by using a detection efficiency defined differently, defining DE as the history independent probability that an APD will produce an electrical pulse given one photon incident on its surface. By "history independent," we mean that the resulting DE is an average DE at a particular mean incident photon rate. We denote this (count-rate-dependent) efficiency by $\eta|_{\text{countrate}}$. This definition of DE decreases the number of APD effects to be independently characterized. It is obvious that the deadtime effect is folded into the definition of $\eta|_{\text{countrate}}$, so deadtime does not need to be measured separately. More importantly, the twilight characteristics such as twilight DE and time constants need not be established separately. However, the fraction of afterpulses due to electronics must still be

measured to apply necessary corrections. We see that if $\eta|_{countrate}$ of the APD is measured at a given count rate, we need much less information about the APD, which decreases the uncertainty associated with independent measurements of APD's properties and helps to establish radiant power with higher accuracy. This is particularly useful when the radiant power of the source is measured simultaneously with the APD coincidence pair calibration technique.

This highlights the fact that because of the complicated nature of photon-counting detectors, the appropriate definition of DE often depends on the particular application. As another example, consider the application that ignores delayed detections, such as the fast quantum communication channel. The DE definition for this application must reflect this condition and establish the DE with an appropriate cutoff of the 10 ns tail.

3.2 Conversion of a photon rate to radiant power

To compute radiant power from the rate of detection of single photons, one needs to know the spectrum of detected signal. We independently measured the transmittance of the narrow-band DUT filter, $T_{F_{DUT}}$, and checked that the spectrum of the down-converted light did not differ significantly from a white light source. We then calculated an average energy per photon:

$$
E = \frac{hc \int_{-\infty}^{\infty} \left(T_{F_{DUT}}(\lambda) / \lambda \right) d\lambda}{\int_{-\infty}^{\infty} T_{F_{DUT}}(\lambda) d\lambda},
\tag{4}
$$

where h is Plank's constant and c is the speed of light. $T_{F_{DUT}}$ (Fig. 8) was measured independently on the NIST facility for Spectral Irradiance and Radiance Responsivity Calibrations using Uniform Sources (SIRCUS) [19] with an absolute uncertainty of 0.1 %. Two measurements taken in one day with a 1 hour interval are presented in fig. 8.
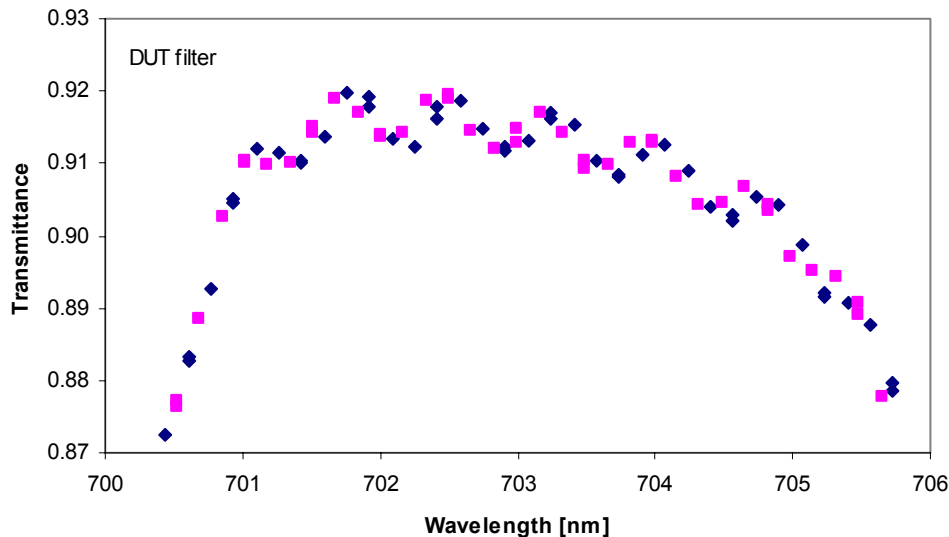
Fig. 8. Transmittance spectra of filter $T_{F_{DUT}}$ measured with SIRCUS. Shown are the two measurements (squares, diamonds) taken on a same day ~1 hour apart.

Note here that the fringe on top of the spectrum shifts throughout the day, presumably due to thermal effects. We found that the resulting DE uncertainty in calculating E due to a shifting fringe was less than 0.1 %.

Finally, if $\eta|_{\text{countrate}}$ is known (see 3.1), we can find the radiant power as:

$$P = \eta|_{\text{countrate}} E \left(N_{\text{total}} - N_{\text{dark}} - f_{\text{afterpulse}} N_{\text{total}} \right) \big/ t ,\tag{5}$$

where N_{total}, N_{dark} are the measured total count and darkcount values during the time t and $f_{\text{afterpulse}}$ is the fraction of ordinary afterpulse counts. If $\eta|_{\text{countrate}}$ is not known, one should use:

$$P = \eta_{\text{live}} E \frac{\left(N_{\text{total}} - N_{\text{dark}} - f_{\text{afterpulse}} N_{\text{total}} \right)}{t - N_{\text{total}} \left(\tau_{\text{dead}} - \frac{1}{\eta_{\text{live}}} \int_0^{\tau_{\text{dead}}} \eta_{\text{twilight}} \left(\tau \right) d\tau \right)} ,\tag{6}$$

where τ_{dead} is deadtime, and η_{twilight} is a DE of twilight events which varies with time within a deadtime of the detector. Eq. (6) shows that ignoring the twilight properties leads to count-rate-dependent overestimation of radiant power.

Radiant power measured using this technique can be compared with the power measured by a transfer detector via the detector substitution method. The transfer detector should be independently calibrated. In our case, the transfer detector calibration is traceable to the US national standard (NIST High Accuracy Cryogenic Radiometer) [20].

4. HIGH ACCURACY SPD CALIBRATION WITH A CORRELATED PHOTON METHOD

To measure the SPD DE (as defined in section 3.1) to high accuracy using a correlated photon method one needs to determine the number of coincidences N_{c} and a number of trigger detections N_{trig}. The DE of the SPD DUT channel is $\eta_{\text{DUTchan}}|_{\text{countrate}} = \eta|_{\text{countrate}} \eta_{\text{channel}} = N_{\text{c}} / N_{\text{trig}}$, where η_{channel} represent all the propagation losses of the DUT channel before an APD. The number of coincidences N_{c} can be deduced from features A and B of the processed histogram, Fig. 3. An accurate determination of N_{trig} requires the electronic detector pulses to be summed during the counting period, and the corrections applied. Corrections involve darkcounts and counts due to background photons, which can be independently measured. Other corrections deal with a complex response function of the SPD and its electronics as well as the pulse and coincidence counting electronics. These corrections require estimates of quantities such as the fraction of afterpulses in the trigger arm, double reflection of the fiber link that delays the trigger pulse resulting in a reduction of the main coincidence peak, and the number of histogram measurements that are cut short due to a retriggering of the start channel. Experimental techniques for estimating some of these corrections are reviewed in Ref. [21]. Note that because the trigger SPD is similar to SPD DUT, and hence has similar properties such as count-rate-dependent afterpulsing, twilight detections etc., it must be characterized independently. The trigger characterization is similar to one just described. In our case, with trigger rates of ≈10 kHz, most of these effects are negligible. However, we stress the necessity to consider systematic uncertainties associated with neglecting these effects in every calibration setup. Finally, to extract the detection efficiency of the SPD $\eta|_{\text{countrate}}$ from the detection efficiency of the entire DUT channel $\eta_{\text{DUTchan}}|_{\text{countrate}}$ one must determine η_{channel} which consists of: the Fresnel reflectance loss of the output surface of the PDC crystal, the loss of F_{DUT}, the loss of the lens [21], and the loss due to finite size of the aperture. Note that the insertion loss due to F_{DUT} depends on spectral distribution of the correlated photons, which is related to the filter F_T via the energy conservation constraint of the downconversion phenomenon [21, 23].

To find η_{live} one needs to perform additional measurements of the SPD DUT, because η_{live} can not be measured directly. In particular we need to establish τ_{dead} and η_{twilight} (with associated uncertainties) using techniques described above, then η_{live} is:

$$\eta_{\text{live}} = \eta\big|_{\text{countrate}} \left(t - N_{\text{total}} \left(\tau_{\text{dead}} - \frac{1}{\eta_{\text{live}}} \int_0^{\tau_{\text{dead}}} \eta_{\text{twilight}}(\tau) d\tau \right) \right) t^{-1}. \tag{7}$$

We see that η_{live} is determined with less accuracy than $\eta\big|_{\text{countrate}}$. In principle, one could use feature (B), separated from feature (A) (fig. 3) to calculate $\eta_{\text{twilight}}(\tau)$, however the accuracy of this estimate would be poor. For cw applications, we could instead estimate the value of the whole integral by calculating $\eta\big|_{\text{countrate}}$ at different count rates and choose the value of the integral to best satisfy $\eta_{\text{live}} = const$.

5. CONCLUSIONS

We have given an overview of techniques and algorithms for measurement of complex effects of SPDs and shown that the characterization of such properties is essential for a high accuracy calibration of SPDs by either conventional substitution, or by correlated photon pair methods. In particular, we showed how to measure "basic" properties of the SPDs such as deadtime, together with lesser known features such as twilight detection, and count-rate-dependent afterpulsing. We outlined how to measure radiant power with an SPD with high accuracy given various definitions of SPD DE. The results of this work have been directly applied to an independent verification of the correlated photon pair calibration technique at NIST. Moreover, because this study highlights a wide range of SPD properties, the results are applicable to other projects involving SPDs (such as high speed quantum networks which have requirements for timing jitter, fidelity, and transfer rate). These results can also be useful in providing ways to overcome the negative effects of these SPD properties in specific applications.

REFERENCES

1. Quinn, T. J., 1997, Metrologia, **34**, 61-65
2. Louisell, W. H., Yariv, A., and Siegman, A. E., 1961, Physical Review, **124**, 1646–1654.
3. Zernike, F. and Midwinter, J. E., 1973, Applied Nonlinear Optics, (New York: Wiley).
4. Burnham, D. C. and Weinberg, D. L., 1970, Physical Review Letters, **25**, 84–87.
5. Klyshko, D. N., 1977, Soviet Journal of Quantum Electronics, **7**, 591–594.
6. Klyshko, D. N., 1981, Soviet Journal of Quantum Electronics, **10**, 1112–1116.
7. Malygin, A. A., Penin, A. N., and Sergienko, A. V., 1981, Soviet Journal of Quantum Electronics, **11**, 939–941.
8. Bowman, S. R., Shih, Y. H., and Alley, C. O., 1986, The use of geiger mode avalanche photodiodes for precise laser ranging at very low light levels: An experimental evaluation, Proceeding of SPIE, **663**, 24–29.
9. Rarity, J. G., Ridley, K. D., and Tapster, P. R., 1987, Applied Optics, **26**, 4616–4619.
10. Penin, A. N. and Sergienko, A. V., 1991, Applied Optics, **30**, 3582–3588.
11. Ginzburg, V. M., Keratishvili, N., Korzhenevich, E. L., Lunev, G. V., Penin, A. N., and Sapritsky, V., 1993, Optical Engineering, **32**, 2911–2916.
12. Kwait, P. G., Steinberg, A. M., Chiao, R. Y., Eberhard, P. H., Petroff, M. D., 1994, Applied Optics, **33**, 1844–53.
13. Migdall, A., Datla, R., Sergienko, A., Orszak, J. S., and Shih, Y. H., 1995/6, Metrologia, **32**, 479–483.
14. Brida, G., Castelletto, S., Degiovanni, I. P., Novero, C., and Rastello, M. L., 2000, Metrologia, **37**, 625–628.
15. Brida, G., Castelletto, S., Degiovanni, I. P., Genovese, M., Novero, C., and Rastello, M. L., 2000, Metrologia, **37**, 629–632.
16. Ware, M., Migdall, A. L., Bienfang, J. C., and Polyakov, S. V., "Calibrating photon-counting detectors to high accuracy: background and deadtime issues", Journal of Modern Optics, to appear

17. M. Ghioni and G. Ripamonti, 1991, Rev. Sci. Instrum., **62**, 163.
18. Wu, L., Chen, X., Zhai, Y., and Zang, D., 2006, SPIE Optics & Photonics, San Diego, CA.
19. Brown, S. W., Eppeldauer, G. P., and Lykke, K. R., Applied Optics, to appear
20. Larason, T. C., Bruce, S. S., and Parr, A. C., Spectroradiometric Detector Measurements, Part 1–Ultraviolet Detectors, and Part 2–Ultraviolet and Visible to Near-Infrared Detectors, NIST Special Publication 250-41
21. Migdall, A. L., 2001, IEEE Transactions on Instrumentation and Measurement, **50**, 478–481.
22. Cheung, J., Gardner, J., Migdall, A. L., Polyakov, S. V., and Ware, M., to be published
23. Polyakov, S. V. and Migdall, A. L., to be published